International Journal of Nanomedicine

Dovepress
open access to scientific and medical research

Open Access Full Text Article

ORIGINAL RESEARCH

Small molecules modified biomimetic gelatin/hydroxyapatite nanofibers constructing an ideal osteogenic microenvironment with significantly enhanced cranial bone formation

This article was published in the following Dove Press journal:
International Journal of Nanomedicine

Daowei Li[1,2]
Kai Zhang[2]
Ce Shi[1,2]
Lijun Liu[1]
Guangxing Yan[1]
Cangwei Liu[1]
Yijun Zhou[1]
Yue Hu[1]
Hongchen Sun[3]
Bai Yang[2]

[1]Department of Oral Biology, Jilin Provincial Key Laboratory of Tooth Development and Bone Remodeling, School and Hospital of Stomatology, Jilin University, Changchun, People's Republic of China; [2]Department of Oral Pathology, Liaoning Province Key Laboratory of Oral Disease, School and Hospital of Stomatology, China Medical University, Shenyang, People's Republic of China; [3]Department of Multiscale Diagnosis and Treatment Chemistry, State Key Laboratory of Supramolecular Structure and Materials, College of Chemistry, Jilin University, Changchun, People's Republic of China

Correspondence: Hongchen Sun
Liaoning Province Key Laboratory of Oral Disease, School and Hospital of Stomatology, China Medical University, No. 117 Nanjing North Street, Heping District, Shenyang 110002, People's Republic of China
Tel +86 24 3132 9999
Fax +86 24 3192 7811
Email hcsun@jlu.edu.cn

Background: Repair of nonunion critical-sized bone defects is a significant clinical challenge all over the world. Construction of osteogenic microenvironment that provides osteoconductive and osteoinductive signals is a leading strategy.

Materials and methods: In the present study, ascorbic acid (AA) and β-glycerophosphate disodium salt hydrate (β-GP) modified biomimetic gelatin/hydroxyapatite (GH) nanofibrous scaffolds were developed by electrospinning. Then the scaffolds were crosslinked by N-hydroxysulfosuccinimide sodium salt (NHS) and 1-(3-Dimethylaminopropyl)-3-ethylcarbodiimide hydrochloride (EDC). The morphology of the non-crosslinked and crosslinked scaffolds was evaluated by scanning electron microscope (SEM). Fourier transform infrared spectroscopy (FT-IR) was used to assess the interacting model between the small molecules and GH scaffold. Then MTT, Alamar Blue, and CCK8 assays were used to investigate the biocompatibility of the various crosslinked scaffolds. Subsequently, the osteogenic genes expression of bone marrow stromal cells (BMSCs) cultured on the scaffolds were detected by quantitative reverse transcription polymerase chain reaction (qRT-PCR). Finally, the crosslinked scaffolds were implanted in a rat calvarial defect model to assess the osteogenic effects in vivo.

Results: SEM results showed that the various scaffolds presented extracellular matrix (ECM)-like fibrous porous structure. (FT-IR) spectrum indicated that AA and β-GP were covalently bonded with GH scaffolds. The MTT, Alamar Blue, and CCK8 assays demonstrated that all the scaffolds can support BMSCs' growth well. The qRT-PCR results showed that the expression level of *Alp* and *Runx2* in BMSCs on GH/A/B scaffold was about 3.5- and 1.5-fold, respectively, compared with that of GH group on day 7. The results also showed that AA- and β-GP-modified GH scaffolds can significantly induce the higher levels of osteogenic gene expression in a temporal specific manner. Importantly, AA and β-GP synergistically promoted osteoblast differentiation in vitro and dramatically induced bone regeneration in vivo. Impressively, AA and β-GP dual modified GH nanofibrous scaffold could serve as a template for guiding bone regeneration and the bone defects were almost repaired completely (94.28%±5.00%) at 6 weeks. Besides, single AA or β-GP-modified GH nanofibrous scaffolds could repair 62.95%±9.39% and 66.56%±18.45% bone defects, respectively, at 12 weeks in vivo. In addition, AA and β-GP exhibit an anti-inflammatory effect in vivo.

Conclusion: Our data highlighted that, AA, β-GP, and GH nanofibers created a fine osteoconductive and osteoinductive microenvironments for bone regeneration. We demonstrated that AA and β-GP dual modified GH nanofiber is a versatile bone tissue engineering scaffold.

Keywords: microenvironment, bone tissue engineering, β-glycerophosphate disodium salt hydrate, ascorbic acid, gelatin, hydroxyapatite nanofibers

submit your manuscript | www.dovepress.com
Dovepress
http://dx.doi.org/10.2147/IJN.S174553

Introduction

Repair of nonunion critical-sized bone defects is a clinically significant challenge all over the world, because the gap between the broken ends of bone is too large leading to poor osteoconductive and osteoinductive microenvironments. Thus, it is critical to develop a method to rebuild such microenvironment for bone regeneration.[1] Recently, bone tissue engineering provides a good solution for repairing large bone defects by interdisciplinary approaches.[2] However, the effect of osteogenesis still needs to be improved. One critical strategy is to construct a biomimetic microenvironment, which provides osteoconductive and osteoinductive signals.[3,4] The physiological microenvironment is a very complicated network, composing of extracellular proteins, proteoglycans, soluble biochemical molecules, etc., which can be described as a collective body of biological and chemical factors surrounding and affecting cells.[5] The microenvironment is tissue specific and even cell-type specific. Thus, the creation of a pro-osteogenic microenvironment is critical for bone regeneration.

Extracellular matrix (ECM) is one of the primary components of bone microenvironment. Besides, ECM can provide structural support that spatially and temporally regulates cell behavior. The ECM has multiple effects beyond providing structural support, such as ECM proteins can bind integrins on the cell surface and transduce environmental signals into cells.[5] Bone tissue engineering scaffolds are typically designed based on native bone ECM structure and composition. A variety of scaffolds have been designed as bone ECMs substitutes, eg, hydrogels,[6] phase separation nanofibrous scaffolds,[7] 3D printing scaffolds,[8] and electrospun nanofibrous scaffolds.[9] Among them, electrospun nanofibrous scaffolds have gained great attention due to their natural ECM-like architecture, easy to fabricate, and low cost.[10]

Many natural and synthetic macromolecules have already been made into nanofibers through electrospun method.[10] Compared with synthetic polymers, natural polymeric electrospun nanofibrous scaffolds are much more similar with natural ECM in terms of structure and composition. Bone has a hierarchical structure composed of a mineral phase (hydroxyapatite [HA]) and an organic phase (90% type I collagen).[11] Thus, collagen (or gelatin [Gel]) and HA are ideal candidates for mimicking bone ECM and the nanofibrous scaffolds based on them would provide an osteogenic microenvironment. Studies have indicated that electrospun Gel/HA (GH) nanofibers can promote ALP activity and osteocalcin expression in osteoblasts in vitro.[12,13] Besides, Gel or HA is also widely used to enhance the biocompatibility of synthetic polymers based electrospun nanofibers, such as poly(lactic-co-glycolic acid) (PLGA),[14] poly(lactic acid) (PLA),[15] and poly-caprolactone (PCL),[16] in our group and other research groups. Thus, electrospun GH nanofibers are excellent candidates for rebuilding osteogenic ECM microenvironment in vivo.

Growth factor is another important component in bone tissue engineering for creating osteogenic microenvironment such as BMP2.[17–19] However, high costs, structural integrity requirements, and unwanted immunogenic responses reduce their potential clinical applications.[19] New strategies applying inexpensive small molecules such as simvastatin,[20,21] vitamin D,[22] bisphosphonate,[23] ascorbic acid (AA), and β-glycerophosphate disodium salt hydrate (β-GP)[24] can obviate these problems. Among them, AA and β-GP are widely used to induce osteoblast differentiation in vitro. Studies have proved that AA acts as a cofactor in the posttranslational modification of collagen and increases collagen production.[25] In terms of β-GP, it can provide sufficient inorganic phosphate under the activity of ALP.[26] Inorganic phosphate is an important element in the mineralization of bone. Multiple genes associated with osteoblast differentiation are regulated by phosphate.[27] Moreover, β-GP displays synergistic actions with AA to stimulate collagen accumulation and ALP activity in differentiated osteoblast-like cells.[26,28] Thus, AA and β-GP are excellent candidates in creating an osteogenic microenvironment.

In view of the thought upward, the combination of ECM-like GH nanofiber, AA and β-GP should create a strong osteogenic microenvironment for bone regeneration. Herein, we created novel AA- and β-GP-modified GH electrospun nanofibrous scaffolds and examined osteogenic activity in vitro and in vivo. We found that our newly developed scaffolds could notably induce new bone formation notably by providing versatile osteoconductive and osteoinductive microenvironments for osteoblasts' differentiation. Our findings provide a new strategy to manage large-sized bone defects in future clinical application.

Materials and methods

Materials

AA, β-glycerophosphate disodium salt hydrate (β-GP), NH, EDC, 1,1,1,3,3,3-hexafluoro-2-propanol (HFIP), nano-HA powder (HA, diameter less than 200 nm), and Gel (type A) were purchased from Sigma Aldrich Co. (St Louis, MO, USA).

Preparation and characterization of the scaffolds

GH, GH/AA (GH/A), GH/β-GP (GH/B), and GH/AA/β-GP (GH/A/B) nanofibrous scaffolds were fabricated via

electrospinning as described in our previous studies.[14,21] Briefly, (1) GH electrospun solution was prepared by dissolving 0.1 g of HA in 3 mL of HFIP under magnetic stirring for 24 hours; meanwhile, 0.9 g of Gel was added to 7 mL of HFIP under magnetic stirring for 24 hours to get a uniform solution; then, the two solutions were mixed together and stirred for over 48 hours to get GH electrostatic spinning solution; (2) GH/B, GH/A, and GH/A/B electrostatic spinning solutions were prepared based on the above solution. GH/B solution was prepared by adding 432 mg of β-GP into the prepared GH solution, whereas GH/A solution was prepared by adding 40 mg of AA into the prepared GH solution. For preparing GH/A/B solution, 432 mg of β-GP and 40 mg of AA were simultaneously added into the prepared GH solution. The mixtures were stirred for another 12 hours. Then, the solutions were electrospun at 15 kV of high voltage to obtain nanofibrous scaffolds.

Cross-linking of collagen- and Gel-based scaffolds with EDC and NHS has been reported by many literatures.[29,30] In our current study, we created a modified method to maintain the topological structure. First, cross-linking agent was made by dissolving 0.115 g of NHS and 0.119 g of EDC in 100 mL of 95% acetone. Then, this solution was cooled down to −20°C. The four kinds of electrospun scaffolds were immersed in the cross-linking agent at −20°C for 12 h, followed by another 0.5 hour at room temperature. After that, the cross-linked scaffolds were rehydrated by a serious of gradient concentration of acetone solution (90, 70, 50, 30, and 10%, respectively) and pure water per 5 minutes at 4°C. Finally, the scaffolds were lyophilized and kept at room temperature. Scanning electron microscopy (SEM; FESEM 6700F; JEOL, Tokyo, Japan) was performed to examine the surface morphology of the scaffolds. To verify the chemical composition and the intermolecular interaction among various components of the various scaffolds, Fourier-transform infrared spectroscopy (FT-IR) (Bruker Optics Inc, Billerica, MA, USA) was performed over a range of 500–4,000/cm. All spectra were recorded by transmittance mode.

Cell culture

Animal use in this study was approved by Jilin University Animal Care and Use Committee. The animal experiments were carried out in accordance with requirements of the m Experimental Animal Ethics and Welfare guidelines (Permit Number: 201611). Rat bone marrow stromal cells (BMSCs) were isolated from femurs of 4-week-old rats. Briefly, bone marrow cells were flushed out using a 20 mL syringe and plated in a 25 mL cell culture flask (NEST, Wuxi, China). The cells were cultured in low-glucose DMEM (L-DMEM; Thermo Fisher Scientific, Waltham, MA, USA) supplemented with 10% FBS, 100 mg/mL of streptomycin (Thermo Fisher Scientific), and 100 U/mL of penicillin (Thermo Fisher Scientific) at 37°C in a 5% CO_2 incubator. The medium was changed after 4 days of isolation of cells, and then the culture medium was changed every 3 days. The third passage of BMSCs was prepared for subsequent tests.

Cell viability and proliferation assay

Cell viability and proliferation was tested by the MTT (AMRESCO, USA) assay. To place the scaffolds (GH, GH/A, GH/B, and GH/A/B) into the wells of 96-well plate, scaffolds were cut into circular shape with a diameter of 6.3 mm. The scaffolds were sterilized using ultraviolet light for 1 hour for each side. Then, the scaffolds were placed into the wells of 96-well plate and secured with a stainless-steel ring. BMSCs were seeded onto the scaffolds at a density of 1×10^4 cells/cm^2. MTT assay was performed on 1, 3, and 5 days after culture. Briefly, 20 μL of MTT solution was added to each well and, then, incubated at 37°C for 4 hours. After that, the supernatant was discarded and the precipitated formazan crystal was dissolved by dimethyl sulfoxide (DMSO). The formazan solution was pipetted into a new 96-well plate, because of the opacity of the scaffolds. Finally, the absorbance was detected by a microplate reader (RT-6000; Lei Du Life Science and Technology Co, Shenzhen, China) at 490 nm wavelength. Furthermore, Alamar Blue (AB) assay was used to quantitatively measure the proliferation of BMSCs. Briefly, BMSCs were cultured on scaffolds as described earlier and 150 μL of culture medium was added to each well. Subsequently, 5 μL of AB solution (Solarbio, Beijing, China) was added to the well and then the cells were incubated for another 7 hours at 37°C in the incubator. After that, 100 μL of the cell culture supernatant of each well was transferred to a new 96-well plate. Fluorescence measurements were carried out at an excitation wavelength of 530±25 nm and an emission wavelength of 590±35 nm. Scaffolds without cells were performed as blank control.

To further evaluate the effects of various scaffolds on BMSCs' viability, cell counting kit 8 (CCK8) and AB assays were used. In brief, sterile 20 mg of various scaffolds were immersed in 2 mL of culture medium without FBS followed by a 5-day incubating period at 37°C. Then, the medium as well as a serious of dilutions (2, 5, and 10 times diluted) were used to culture cells after adding 10% FBS. The medium incubated in 37°C without scaffold was used as control for culturing cells after adding 10% FBS. In the experiments, the BMSCs were seeded into 96-well plates at a density of 0.5×10^4 cells/well. Then, 100 μL of various elutions

were added into each well and the cells were incubated at 37°C for 24 hours before investigation. Before performing CCK8 assay, the medium was replaced by fresh L-DMEM first and then 10 μL of CCK8 solution was added to each well followed by a 3-hour incubation at 37°C. Finally, the absorbance was detected by a microplate reader (RT-6000; Lei Du Life Science and Technology Co, Shenzhen, China) at 450 nm wavelength. For AB assay, the medium was also replaced by fresh L-DMEM first and, then, 5 μL of AB solution (Solarbio) was added to each well followed by a 7-hour incubation at 37°C. Subsequently, 100 μL of the cell culture supernatant of each well was transferred to a new 96-well plate for fluorescence measurements, which were carried out at an excitation wavelength of 530±25 nm and an emission wavelength of 590±35 nm. Scaffolds without cells were performed as blank control.

Quantitative reverse transcription PCR (qRT-PCR)

Circular scaffolds with a diameter of 10.2 mm were placed in 24-well plates and secured with a matched stainless-steel ring. BMSCs were seeded at a density of 1×10^5 cells/well. The medium was changed every 3 days. Total mRNA was extracted on 7 and 14 days after culture using a Qiagen RNeasy mini purification kit (Qiagen NV, Venlo, the Netherlands). Full-length cDNA was reverse transcribed using an iScript™ cDNA synthesis kit (Takara Bio, Dalian, China). The expressions of osteoblastic marker genes *Runx2*, *Alp*, type I collagen (*Col1*), and *Sp7* were examined by qRT-PCR (MxPro Mx3005P; Agilent Technologies, Santa Clara, CA, USA) using SYBR-Green premix Ex Taq kit (Takara Bio). Housekeeping gene β-actin was used as the internal control. The primers used for this analysis are listed in detail in Table 1. Primers were synthesized commercially (Takara Bio).

Table 1 The primer sequences used for qRT-PCR

Genes	Forward sequence/reverse sequence
β-actin	5′-GGAGATTACTGCCCTGGCTCCTA-3′/ 5′-GACTCATCGTACTCCTGCTTGCTG-3′
Col1	5′-GACATGTTCAGCTTTGTGGACCTC-3′/ 5′-AGGGACCCTTAGGCCATTGTGTA-3′
Runx2	5′-CATGGCCGGGAATGATGAG-3′/ 5′-TGTGAAGACCGTTATGGTCAAAGTG-3′
Alp	5′-CATCGCCTATCAGCTAATGCACA-3′/ 5′-ATGAGGTCCAGGCCATCCAG-3′
Sp7	5′-AAGTTATGATGACGGGTCAGGTACA-3′/ 5′-GAAATCTACGAGCAAGGTCTCCAC-3′

Abbreviation: qRT-PCR, quantitative reverse transcription PCR.

In vivo animal study

Rat calvarial defect model creation and scaffolds implantation

Animal use in this study was approved by Jilin University Animal Care and Use Committee. The animal experiments were carried out in accordance with requirements of the Experimental Animal Ethics and Welfare guidelines (Permit Number: 201611). Thirty 6-week-old male Wistar rats (body weight ~200 g) were used. The animals were randomly divided into five groups (control, GH, GH/A, GH/B, and GH/A/B, for each group, n=6). Prior to operation, the animals were anesthetized using isoflurane and lidocaine. The scalp along the sagittal suture was shaved, and the skin was sterilized with iodine. A 15 mm long incision along the sagittal suture was made, and then, the calvarial bone was exposed by blunt dissection. A 5 mm diameter defect was created using a trephine bur (3i Implant Innovation, Palm Beach Gardens, FL, USA) on left parietal bone. The circular scaffolds of 6 mm diameter were sterilized with UV light for 1 hour for each side and implanted into the bone defects for each group (GH, GH/A, GH/B, and GH/A/B). For the control group, the animals were treated the same but without implantation. The periosteum and the overlying skin were then stitched up using 3–0 nylon suture. Six or 12 weeks postsurgery, the rats were anesthetized and perfused through heart by using 4% paraformaldehyde. The whole calvaria was harvested and further fixed with 4% paraformaldehyde at room temperature for 2 days for the following evaluations.

Radiographic analysis

To assess the new bone formation in the bone defect area, micro-computed tomography (micro-CT) (micro-CT 50; Scanco Medical AG, Bassersdorf, Switzerland) was applied under the fixed conditions (24 kV, 2 mA, 90 seconds). Area of new bone formation and percentage were measured using the Image Processing and Analysis in Java (ImageJ-1.51r; NIH, USA) software.

Histological analysis

After micro-CT scanning, the samples were decalcified in 10% EDTA for 2 months, during which time the 10% EDTA solution was changed every week. The samples were embedded in paraffin and sectioned at a thickness of 5 μm for H&E staining. The H&E staining slides were observed under an optical microscope, and the images were captured under the Olympus microscope BX51 and DP73 CCD Olympus Imaging System (Olympus Corporation, Tokyo,

Japan). Histological evaluation was performed by two independent examiners.

Statistical analysis

Quantitative values were expressed as mean ± SD. Statistical differences were evaluated by one-way ANOVA. Differences were considered statistically significant at $P<0.05$, <0.01, <0.001, or <0.0001 level. The in vitro experiments were repeated three times with triplicates for each experiment.

Results

Characterization of nanofibrous scaffold

GH, GH/A, GH/B, and GH/A/B nanofibrous scaffolds were fabricated via electrospinning. Non-cross-linked and cross-linked nanofibrous scaffolds were examined by SEM. Figure 1 shows that all nanofibrous scaffolds presented randomly oriented morphology. There were some scattered and aggregated nano-HA particles on the surface of the fibers (Figure 1, indicated by black arrows). The diameters of the fibers ranged from nanometers to micrometers. Besides, its dimension span was increased as the addition of AA and β-GP. A considerable amount of small-diameter fibers emerged in GH/A, GH/B, and GH/A/B nanofibrous scaffolds. Additionally, the fiber of GH/B scaffold had some swelling. When cross-linked by NHS/EDC, the morphologies of the scaffolds were maintained well. All the scaffolds had good porosity retention, especially the GH and GH/A scaffolds. However, there was a certain degree of swelling in the GH/B and GH/A/B nanofibers. This is certainly due to the incorporation of β-GP, because only the GH/B and GH/A/B groups were found with certain degree of swelling. This might due to that β-GP has two hydroxyl groups in each molecule, which has strong affinity with water. Besides, the content of β-GP was relatively high in the scaffolds. Thus, it is easy to absorb water when it is prepared. The retention of porous structure would be favorable for the exchange of gas, mineral, nutrients, and metabolic wastes, more importantly for the migration and infiltration of cells.

Chemical characterization of scaffolds as well as pure AA, β-GP, Gel, and HA was conducted using the FT-IR analysis (Figure 2). Each pure substrate showed its characteristic peaks as shown in Figure 2. When these substrates are mixed together, many of the absorption bands were over-lapped. However, the shape, location, and intensity of the peak changed greatly. The spectra of GH scaffold (Figure 2) showed typical amide peaks (amide I peak at 1,568/cm, amide II peak at 1,542/cm, and amide III peak at 1,240/cm).[31] Moreover, the GH scaffold showed typical spectral features in the range of 1,150 and 1,000/cm, which were related to the P–O and *P*=O vibrations of HA.[32]

There were blue shifts of amide peaks in GH scaffold compared with pure Gel, especially for amide I absorption peak (Figure 2 and Table 2), which were probably the results of ionic interactions between the positively charged amino groups of the Gel and the negatively charged phosphate groups of the HA. After cross-linking, the GH scaffold showed the shift of amide peaks to lower wavenumbers (GH-C group), especially for amide II band. These factors are mainly due to the reaction of carboxyl groups of amino acids originated from aspartic acid in Gel (Figure 2 and Table 2).[33]

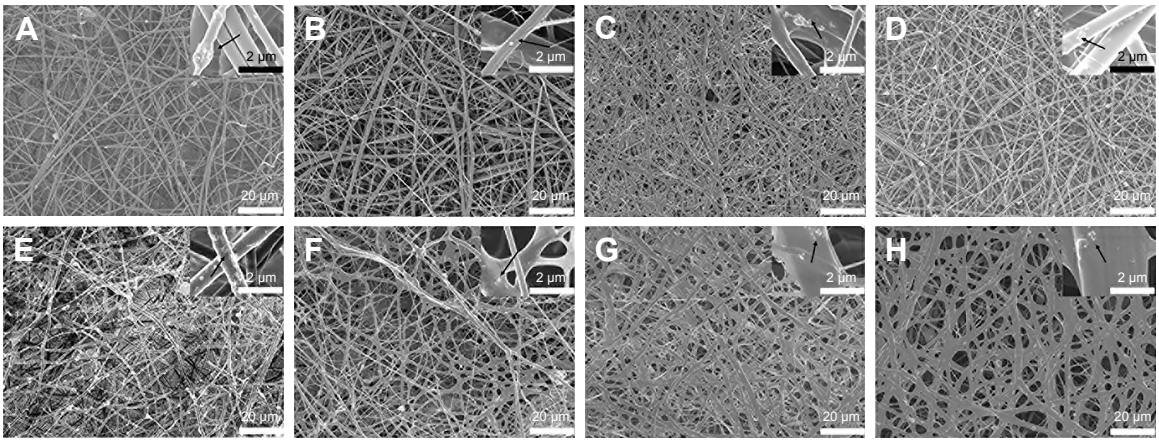

Figure 1 Surface morphology of nanofibrous scaffolds by SEM.
Notes: GH (**A** and **E**), GH/A (**B** and **F**), GH/B (**C** and **G**), GH/A/B (**D** and **H**). Non-cross-linked (**A**–**D**) and cross-linked (**E**–**H**). Black arrow: scattered and aggregated nano-HA particles.
Abbreviations: GH, gelatin/HA; HA, hydroxyapatite; SEM, scanning electron microscopy.

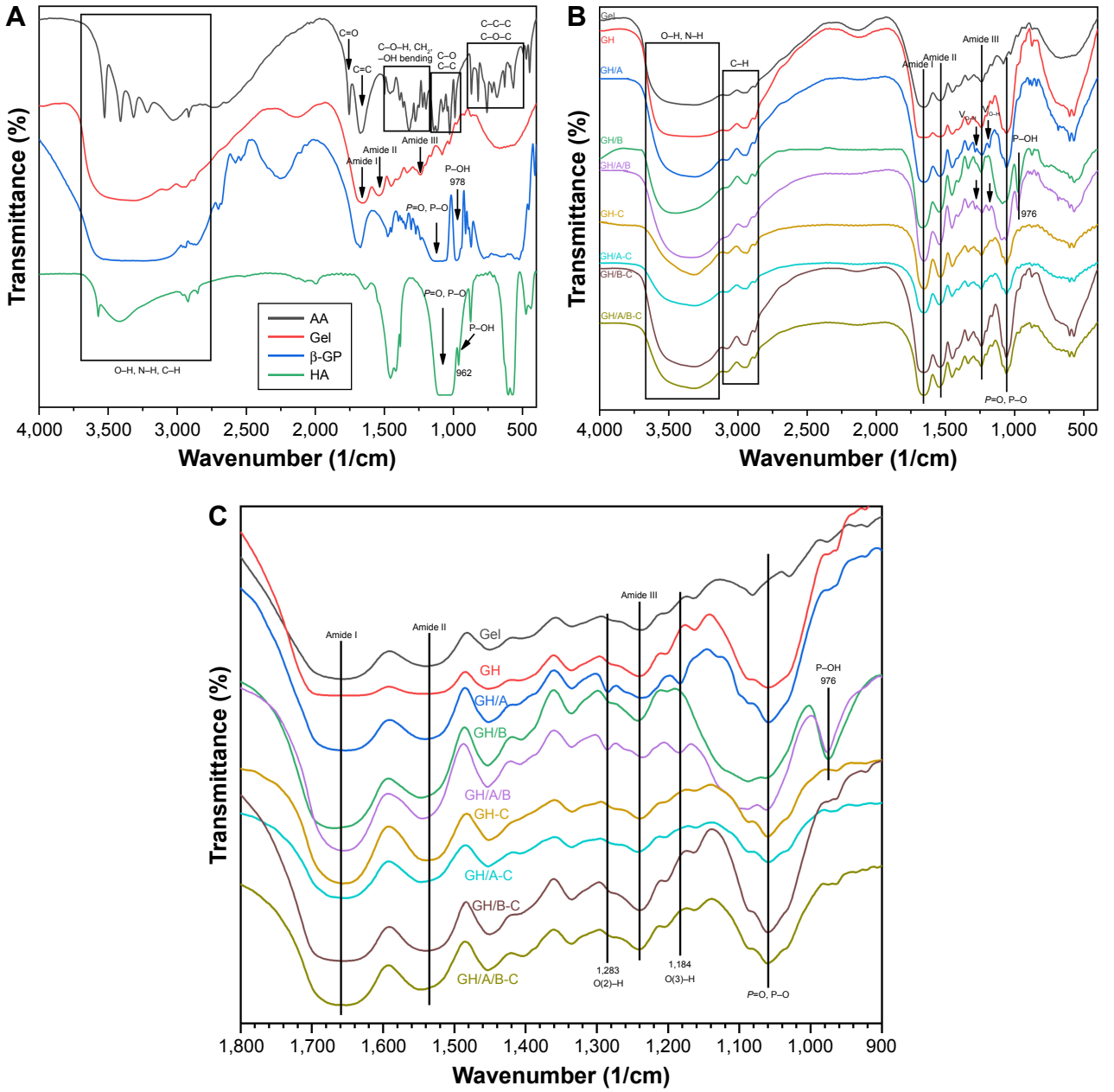

Figure 2 FT-IR spectra in KBr pellets of various scaffolds.
Notes: (**A**) Dried pure AA, β-GP, Gel, and HA, (**B**) various scaffolds, and (**C**) spectra of various scaffolds in the region of 1,800–900/cm. GH-C, GH/A-C, GH/B-C, and GH/A/B-C are indicated as cross-linked GH, GH/A, GH/B, and GH/A/B scaffolds.
Abbreviations: AA, ascorbic acid; FT-IR, Fourier-transform infrared spectroscopy; Gel, gelatin; GH, Gel/HA; HA, hydroxyapatite.

The O–H and N–H bands in the range of 3,650–3,100/cm in the FT-IR spectrum became broader in the GH/A-C group than in the GH-C group. This implied that more –OH and –NH groups were exhibited in the GH/A-C group. There were red shifts of amide absorption peaks in GH/A scaffold compared with GH scaffold, particularly in amide I absorption peak (shifting from 1,658 to 1,650/cm, Figure 2 and Table 2). These results indicated that AA interacts with the C=O, C–N, and N–H groups in Gel and results in the rearrangement of the carbonyl hydrogen and amino hydrogen-bonding network. However, the amide absorption peaks shifted to a higher wavenumber when cross-linked with NHS/EDC (GH/A group compared with GH/A-C group). Nevertheless, the wavenumber of amide I absorption peak in GH/A-C group was still lower than the GH group. Moreover, the spectrum showed that only the amide II peak shifted to higher wavenumber with reduced intensity ratio of A (amide I)/A (amide II) in the GH/A-C group than in the GH-C group. Furthermore, the typical absorption peaks of O(2)–H (1,283/cm) and O(3)–H (1,184/cm)[34] bending

Table 2 Wavelength shifts of amide I, amide II, amide III, and *P*=O/P–O in various scaffolds

	Amide I (1/cm)	Amide II (1/cm)	Amide III (1/cm)	*P*=O/P–O (1/cm)
Gel	1,654	1,541	1,238	
GH	1,658	1,542	1,240	1,059
GH/A	1,650	1,541	1,238	1,059
GH/B	1,668	1,548	1,242	1,088 1,063
GH/A/B-C	1,656	1,545	1,236	1,088 1,063
GH-C	1,656	1,537	1,240	1,061
GH/A-C	1,656	1,546	1,240	1,059
GH/B-C	1,653	1,541	1,240	1,059
GH/A/B-C	1,664 1,655	1,548	1,240	1,061

Abbreviation: GH, gelatin/hydroxyapatite.

mode of AA appeared in the GH/A and GH/A/B groups, while the two peaks disappeared after cross-linking. These results indicated that there was chemical reaction between –O(2)H and –O(3)H within AA and aliphatic amines within Gel, which generated more N–H bonds.[35]

Besides, the spectrum showed that GH/B-C group had a wider absorption band of –OH and –NH stretches compared with the GH-C group. This was mainly due to the large amount of –OH groups in β-GP. In addition, the absorption band of P–O and *P*=O vibrations became broader and shifted to higher wavenumber after adding β-GP. However, absorption band shifted back when cross-linked with EDC/NHS (Figure 2 and Table 2). Moreover, the absorption peak intensity of P–O and *P*=O vibrations were much higher in β-GP containing group after cross-linking. The spectrum also showed that a peak at 974/cm was present in the GH/B and GH/A/B groups, which was related to the P–OH group, while disappeared after cross-linking.[32] These results implied that P–OH group of β-GP could react with amino groups of Gel that generated P–N bond under the catalysis of NHS/EDC.[36]

The effect of scaffolds on the proliferation of BMSCs

Metabolic activity of BMSCs cultured with the scaffolds was evaluated by the MTT assay on 1, 3, and 5 days postculturing (Figure 3). All the scaffolds could support the growth of BMSCs well. There were no significant differences of cell proliferation activity among all the scaffolds. However, cell proliferation on GH scaffold was slightly higher compared with the GH/B group, which indicated that β-GP exhibited an inhibitory effect on cell proliferation. Besides, cell metabolic activity on the GH/A group was a little higher than the GH group; thus, AA can stimulate cell proliferation.

The AB assay has been widely used for the cytotoxicity assay and has high sensitivity. The viabilities of the BMSCs grown on various scaffolds were evaluated using the AB assay during a 5-day period of culturing. Figure 3B displays the AB fluorescence measured on days 1, 3, and 5. The results showed that cell viability, detected by AB assay, had similar tendency with the MTT assay. The cells grown on GH/A and GH/A/B exhibit relatively higher fluorescence intensity than GH and GH/B groups on day 1. Subsequently, the cell viability on the GH and GH/A groups was significantly higher than the GH/B group. With the elongation of time, the cells grown well on all scaffolds. On day 5, the viability of cells grown on GH/A group was significantly higher than the GH/A/B group.

The effects of scaffold elution on BMSCs viability were evaluated by CCK8 and AB assays (Figure 3C and D). The results showed that all the gradient concentration of elution had positive effects on BMSCs' viability. Moreover, the higher concentration of elution was associated with the higher cell activity. There were no significant differences of cell viability among all the scaffolds. Besides, the cell viability on GH/A, GH/B, and GH/A/B groups were relatively higher than GH group in both CCK8 and AB assays. These results demonstrated that various scaffolds had good biocompatibility.

The effect of the scaffolds on osteogenic differentiation of BMSCs

Quantitative PCR was used to quantify the expressions of osteoblastic marker genes (Figure 4). The column chart revealed that the incorporation of AA and β-GP into GH scaffold could increase the expression of *Runx2*, while only increments in the GH/A and GH/A/B groups had statistically significant on day 7 (Figure 4A). Its expression in the GH/A/B group was about 1.5 folds compared to that in the GH group. Furthermore, GH/A/B group induced significantly higher *Runx2* expression when compared with the GH/B group. The expression of *Runx2* could not be detected on day 14 (Figure 4A, indicated as "ND").

As shown in Figure 4B, *Sp7* expression was significantly elevated in the GH/A, GH/B, and GH/A/B groups compared to the GH group on day 7. In addition, the expression of *Sp7* in the GH/A and GH/A/B groups was also significantly higher than in the GH/B group. *Sp7* expression was dramatically upregulated with the doping of AA into scaffolds on day 7.

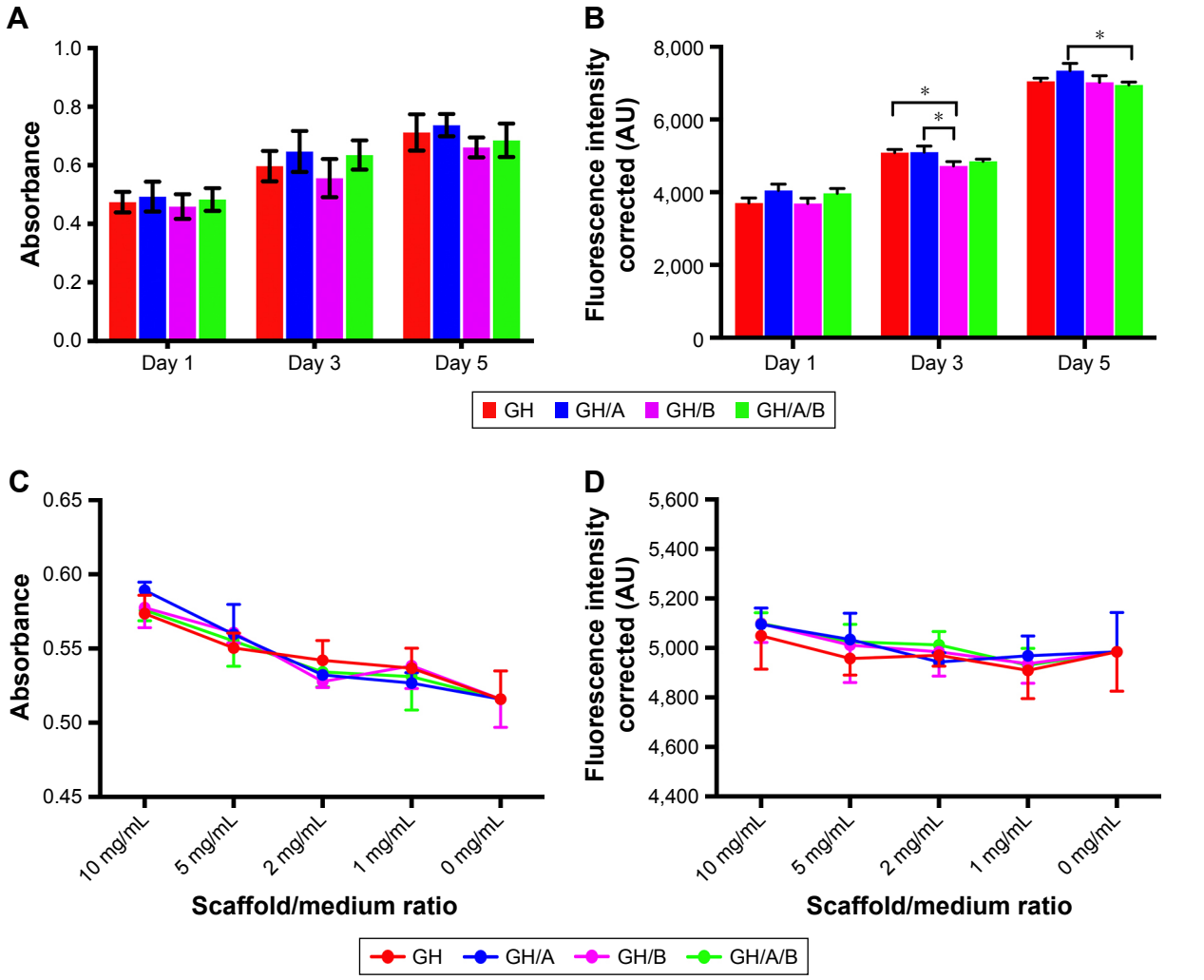

Figure 3 Biocompatibility of various scaffolds.
Notes: Cell viability and proliferation of BMSCs on scaffolds are evaluated through MTT (**A**) and Alamar Blue (**B**) assays. Effects of scaffolds elution on cell viability and proliferation are assessed by CCK8 assay (**C**) and Alamar Blue assay (**D**). Statistically significant differences are marked with an asterisk (*$P<0.05$).
Abbreviations: BMSCs, bone marrow stromal cells; CCK8, cell counting kit 8; GH, gelatin/hydroxyapatite.

Thus, AA revealed more intense effects on *Sp7* expression than β-GP. However, the expression patterns of *Sp7* were markedly changed from day 7 to day 14. Its expression decreased in the GH/A, GH/B, and GH/A/B group compared to the GH group on day 14, especially for the GH/B group. The expression of *Sp7* in GH/B group was significantly lower than the other groups.

In Figure 4C, incorporation of AA or β-GP alone into the GH scaffold (GH/A or GH/B) could also significantly increase *Alp* expression when compared with the GH group. Furthermore, adding both AA and β-GP into GH scaffold (GH/A/B) showed synergistically elevating *Alp* expression on day 7. The expression level of *Alp* in the GH/A/B group was about 3.5-fold that of the GH group on day 7. Whereas, the expression of *Alp* decreased in the GH/A and GH/B groups compared to the GH group on day 14. Moreover, the GH/B group showed a more severe declination of *Alp* expression. However, AA and β-GP showed synergistically effects on the expression of *Alp* in the GH/A/B group, which maintains a relative higher gene expression on day 14. Results showed that expression profile of *Col1* exhibited similar trend as *Alp* (Figure 4D).

The effects of the scaffolds on bone formation in vivo

Osteogenesis of scaffolds was evaluated in a critically sized defects model on rat parietal bone. Micro-CT data clearly showed that there was almost no new bone formation in the control group at 6 weeks postsurgery (Figure 5A). In the GH group, only a very limited amount of new bone was observed at the edge of the bone defect region at 6 weeks postsurgery (Figure 5B). The GH/A or GH/B group showed

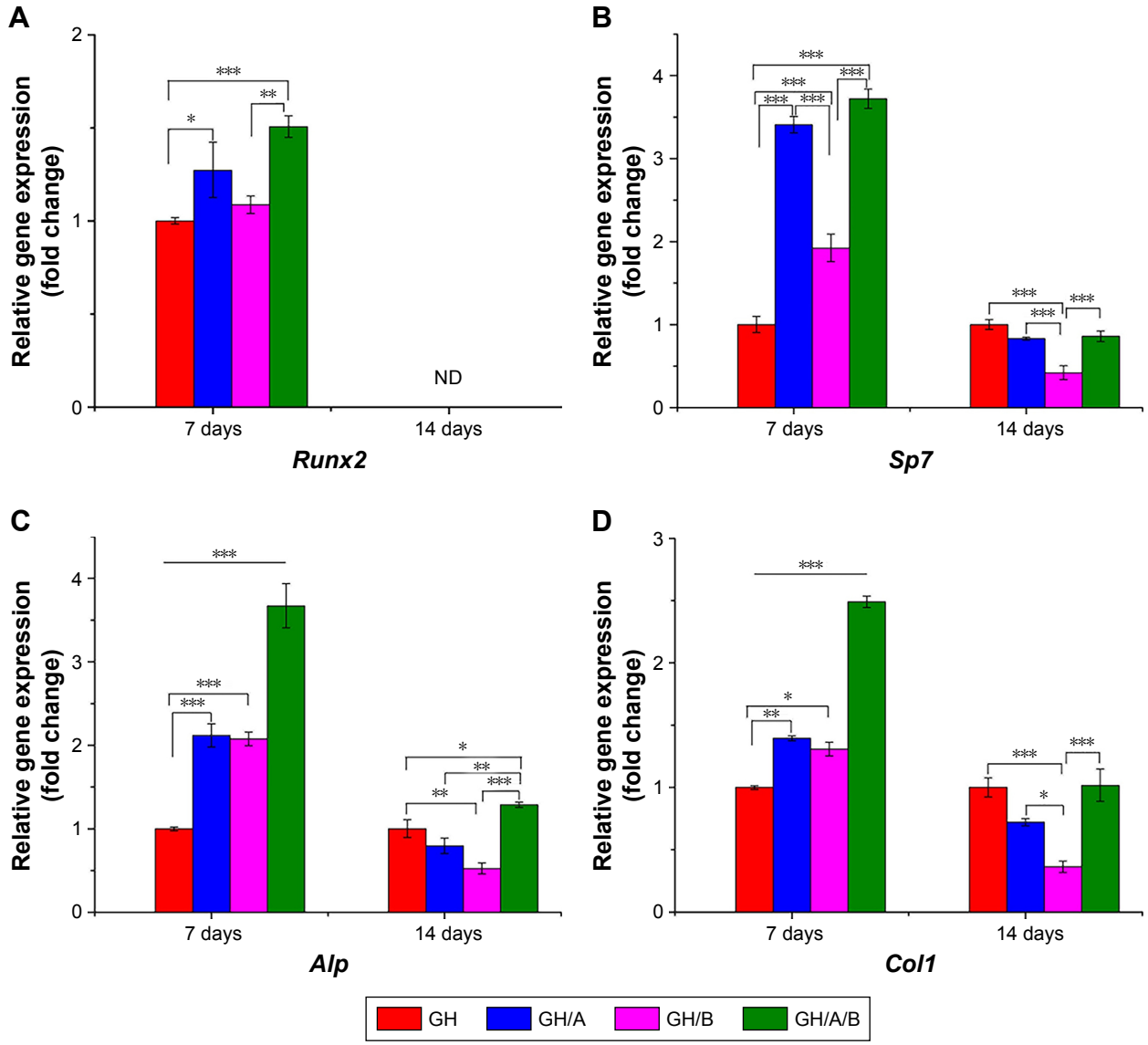

Figure 4 Normalized osteoblastic marker gene expressions of BMSCs on days 7 and 14.
Notes: Relative genes expression (**A**) *Runx2*, (**B**) *Sp7*, (**C**) *Alp*, and (**D**) *Col 1*. Statistically significant differences are marked with an asterisk (*$P<0.05$, **$P<0.01$, ***$P<0.001$). GH, GH/A, GH/B, and GH/A/B: cells cultured on the corresponding scaffolds.
Abbreviations: BMSCs, bone marrow stromal cells; GH, gelatin/hydroxyapatite; ND, not detected.

increased new bone formation compared with the GH group (Figure 5C, D, and K). Moreover, the defect was dramatically repaired in the GH/A/B group as early as 6 weeks postsurgery (Figure 5E and K). Quantified analysis also demonstrated that the percentage of area of new bone formation in the GH/A/B group (94.28%±5.00%) was significantly much more than control (6.65%±2.30%), GH (9.89%±5.96%), GH/A (33.89%±4.07%), and GH/B (33.04%±3.17%) groups (Figure 5K). At 12 weeks postsurgery, the repairing of bone defects was further advanced with the increase in time after implantation. In the control group, regenerated new bone was found at the margin of the defect area at 12 weeks (19.87%±16.88%) (Figure 5F and K). The percentage of area of new bone formation in the GH (46.06%±15.25%), GH/A (62.95%±9.39%), GH/B (66.56%±18.45%), and GH/A/B (95.64%±6.16%) groups were significantly higher compared with the control group (19.87%±16.88%) (Figure 5F–K). The GH/A/B scaffold displayed remarkable osteogenic activity, which almost repaired the bone defect at 12 weeks postimplantation.

Further histological analyses confirmed the markedly new bone formation at 6 weeks in the GH/A/B group. It is worth noting that the ends of GH/A/B scaffold were embedded in the newly formed bone (Figure 6E, red arrows). The new bone was deposited along the surface of GH/A/B scaffold (Figure 6J). The newly formed bone had an immature

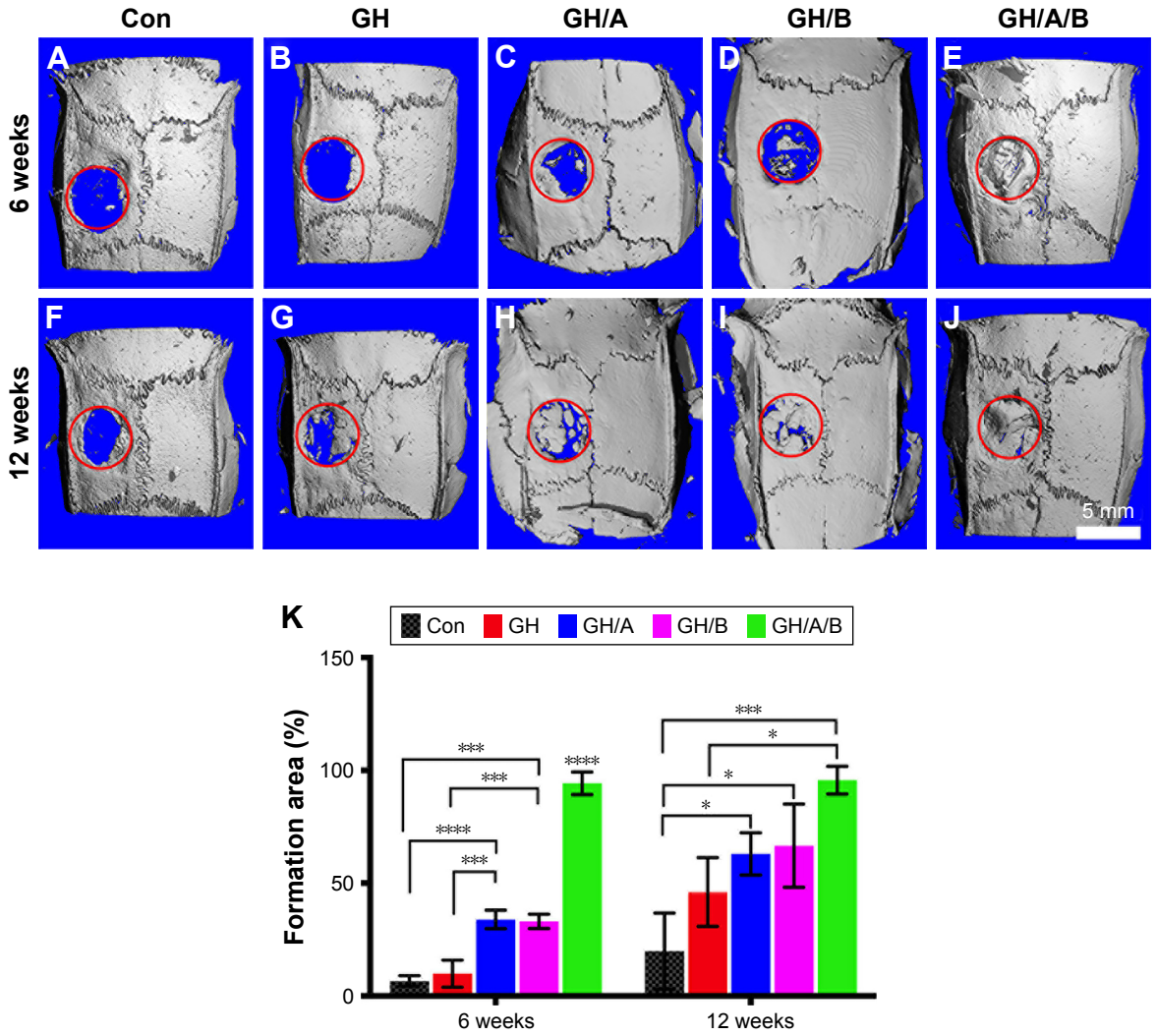

Figure 5 New bone formation at 6 or 12 weeks postsurgery by micro-CT.
Notes: (**A**–**J**) Micro-CT images. (**K**) Percentage of new bone formation was quantified (area of new bone formation/created bone defect). Con: no treatment of bone defect; GH, GH/A, GH/B, and GH/A/B: treatment of bone defect with GH, GH/A, GH/B, and GH/A/B nanofibrous scaffolds, respectively. Statistically significant differences are marked with an asterisk (*$P<0.05$, ***$P<0.001$, and ****$P<0.0001$).
Abbreviations: Con, control; GH, gelatin/hydroxyapatite; micro-CT, micro-computed tomography.

or woven appearance and exhibited embedded osteocytes (Figure 6O). In the control and GH groups, mass fibrous connective tissue grew into the central area of bone defect. Besides, we could find some adipose tissue within the fibrous connective tissue in the GH group. While in the GH/A and GH/B groups, there was a certain amount of new bone deposition in the central areas of the defects. The newly formed bone also had an immature or woven appearance and exhibited embedded osteocytes (Figure 6M and N). Besides, there were some inflammatory cells infiltrating in GH scaffold (Figures 6L and 7L, as indicated by blue arrows). In contrast, there were no inflammatory cells in the GH/A, GH/B, and GH/A/B groups (Figures 6 and 7).

At 12 weeks, histology analyses also revealed that the new bone formation was further increased. The regenerated bone became more mature at 12 weeks (Figure 7). The newly formed bone showed lamellar structure, which was much closer to the native bone (Figure 7M–O). On the contrary, fibrous connective tissue still filled in the central area of defects in the control and GH groups. These results demonstrated that GH/A/B scaffold can provide an excellent microenvironment for osteoblast proliferation and differentiation, which gives rise to rapid new bone formation.

Discussion

Repairing the large bone defects remains a global clinical challenge because of seriously losing osteogenic microenvironment between the broken ends. Microenvironment-based bone tissue engineering strategy provides a good solution for this problem. Herein, we created a unique β-GP- and

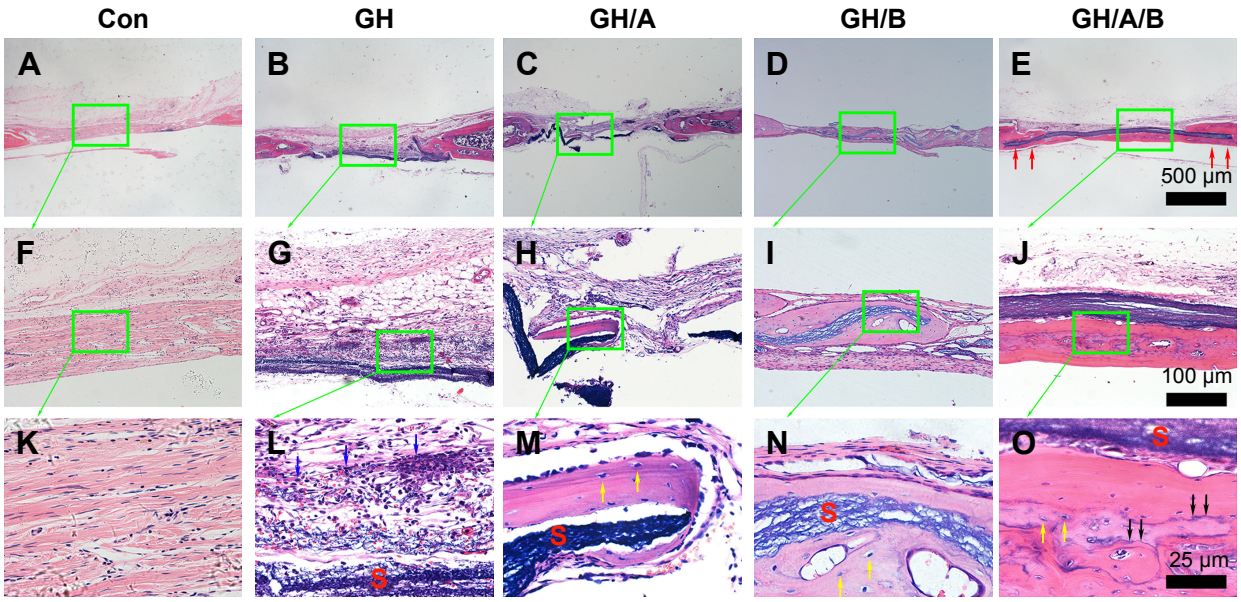

Figure 6 H&E staining of bone defect area at 6 weeks postsurgery.
Notes: (**A**, **F**, and **K**) Con group; (**B**, **G**, and **L**) GH implantation group; (**C**, **H**, and **M**) GH/A implantation group; (**D**, **I**, and **N**) GH/B implantation group; and (**E**, **J**, and **O**) GH/A/B implantation group. S: scaffold remnants; red arrows indicate the ends of GH/A/B scaffolds, which were embedded in the newly formed bone; black arrows: bone deposition line. Yellow arrows: osteocytes embedded in bone matrix. Blue arrows: inflammatory cells. Green rectangular box together with green arrow point to its enlarged image. (**A**–**E**) The same scale bar of 500 μm, (**F**–**J**) the same scale bar of 100 μm, and (**K**–**O**) the same scale bar of 25 μm.
Abbreviations: Con, control; GH, gelatin/hydroxyapatite.

AA-modified biomimetic GH nanofibrous scaffold, which will provide a good osteoinductive and osteoconductive microenvironment to promote osteogenic differentiation and serve as a template to guide osteoblastic lineage cell migration and repairing bone defects. Our data indicate that small molecules in combination with biomimetic scaffolds created by electrospinning techniques provide a well strategy for the treatment of large bone defects.

Newly AA, β-GP, or both modified GH scaffolds were successfully fabricated by electrospinning method. All the

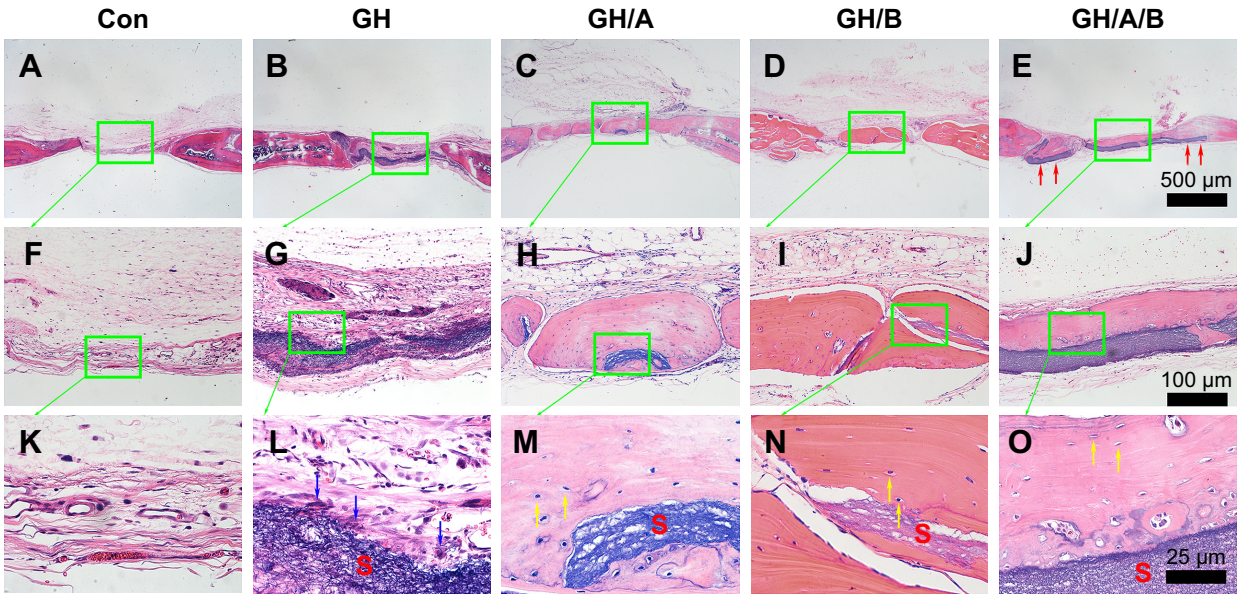

Figure 7 H&E staining of bone defect area at 12 weeks postsurgery.
Notes: (**A**, **F**, and **K**) Con group; (**B**, **G**, and **L**) GH implantation group; (**C**, **H**, and **M**) GH/A implantation group; (**D**, **I**, and **N**) GH/B implantation group; and (**E**, **J**, and **O**) GH/A/B implantation group. S: scaffold remnants; red arrows: the ends of GH/A/B scaffolds were embedded in the newly formed bone; yellow arrows: osteocytes embedded in the bone matrix; blue arrows: inflammatory cells. Each green rectangular box together with green arrow points to its enlarged image. (**A**–**E**) The same scale bar of 500 μm, (**F**–**J**) the same scale bar of 100 μm, and (**K**–**O**) the same scale bar of 25 μm.
Abbreviations: Con, control; GH, gelatin/hydroxyapatite.

scaffolds presented fibrous network structure, and the diameter of the fibers was ranging from nanoscale to microscale. The aggregation of nano-HA on the surface of the fibers might be due to the high viscosity of various blend solutions that contained some aggregated particles. Besides, the applied high-voltage electric field can also drive particles aggregating during electrospinning. However, these aggregated particles may promote osteoblast adhesion, differentiation, and mineral deposition at the mineralization phase of new secreted bone matrix. AA- and β-GP-modified GH nanofibers had larger diameter span than GH fibers maybe due to the increased charge density of the electrospun solution, which could enhance the self-repulsion and the stretching force, while electrospinning. Similar results had been reported by Meng et al[37], who reported that when the Gel was incorporated in PLGA, the diameter distribution became broader, with the increasing of Gel concentration.

It is known that gelatin based nanofibers have poor water resistance and thus will be dissolved in body fluid. Our results showed that the low cross-linking temperature (−20°C) and slow gradient hydration process can better maintain the morphology and structure (Figure 1E–H). This may be due to the low temperature that can make the cross-linking rate at a low level, which can reduce fibers' contraction and swelling of. In contrast, slow gradient hydration process might also reduce the contraction of fibers. We could find that the adding β-GP caused some swelling of fibers in the GH/B and GH/A/B group. This was due to the high content and strong hydrophilicity of β-GP in scaffolds. The retention of fibrous and porous structure would be favorable for cell growth and nutrients and metabolic waste exchange. The FT-IR results indicated that AA and β-GP were covalently bonded with amino acid in Gel. This should significantly improve the duration time and drug effects.

Cell behaviors on the scaffolds are essential for its potential clinical application. Our data indicated that all the scaffolds support BMSCs growth well (Figure 3). Cell proliferation on the scaffolds will reflect the quality of cytocompatible microenvironment of scaffolds. Our results confirmed that GH/A scaffolds can promote BMSCs proliferation slightly, thus improving the cytocompatibility of GH scaffolds. Sufficient cell number is also critical for tissue regeneration that hints the importance of AA in the scaffolds. The AB assay also indicated that the incorporation of AA into scaffolds increased positive effects on cell viability. However, the addition of β-GP into GH scaffolds negatively regulated cell viability, which was seeded on scaffolds. In contrast, the elution of GH/B scaffold had positive effects on cell proliferation based on CCK8 and AB assays. These results implied that the scaffold morphology might significantly affect the cell growth. The SEM images showed that obvious swelling occurred in the GH/B and GH/A/B scaffolds after cross-linking and the diameter of fibers increased significantly, which may not conducive to cell adhesion and proliferation. Studies had shown that cell proliferation on scaffolds could be promoted by regulating the surface topography,[38] such as HA and ion-doped HA could be used to modify scaffolds' architecture and properties, including surface crystallinity, roughness, surface charge, and scaffold rigidity, to promote the osteogenic differentiation of stem cells and bone formation.[39]

Significantly, the created osteogenic microenvironment within scaffolds is critical for generating best repairing effects. AA is required as a cofactor for enzymes that hydroxylate proline and lysine in procollagen,[40] which is critical for forming a proper helical structure of collagen chains. AA enhances the synthesis of collagen matrix at different stages, including gene transcription and protein translation, translation, hydroxylation, and secretion.[41] Our results confirmed that AA can enhance *Col1* expression at RNA level. Apart from collagen matrix synthesis, AA can promote osteoblast differentiation by the activation of osteogenic gene expression, such as *Runx2*, *Alp*, and *Sp7*.[42,43] Therefore, the use of AA in constructing the osteoinductive microenvironment would be an advantage in the treatment of bone-related diseases. Moreover, AA possesses a protective role as an antioxidant and nutritional supplement with no toxic effect.[44] Our results also demonstrated that AA could significantly increase *Runx2*, *Sp7*, and *Alp* expression on day 7 postculturing (Figure 4). However, the promoting effects vanished on day 14. This suggests that AA plays a critical role in the initiation of osteoblast differentiation by activating these osteogenic gene expressions.

A number of studies have suggested that inorganic phosphate is required in the events preceding mineralization.[45] However, contrasting results have brought some debate as to the significance of elevated phosphate in osteoblast differentiation. Studies have reported that phosphate suppressed the expressions of several differentiation markers, ie ALP, osteocalcin, and bone sialoprotein.[46] Furthermore, Okamoto et al[47] indicated that phosphate suppresses osteoblastic differentiation partially through enhancing ROS production in MC3T3-E1 cells. Besides, Beck et al[27] reported that phosphate suppresses the expressions of several matrix proteins including collagen-1α1, 1α2, and decorin but enhanced the expression of another matrix protein, osteopontin. In our

study, the results indicated that β-GP could promote *Alp*, *Sp7*, and *Col1* expressions at 7 days postculturing but significantly suppressed these gene expressions at 14 days postculturing. This implied that the effects of β-GP on osteoblast differentiation is dependent on the stage of osteoblast differentiation, which could be the reason why researchers got contrasting results. The rat primary BMSCs used here are progenitors of skeletal tissue components such as bone, the hematopoiesis-supporting stroma, and adipocytes,[48] while MC3T3-E1 cells are preosteoblast. Thus, we can observe positive regulatory effects of β-GP on osteogenic gene expression in BMSCs, because BMSCs are more primitive than MC3T3-E1 cells. Moreover, the results demonstrated that AA could synergistically act with β-GP to stimulate *Alp* and *Col1* expressions. Thus, the incorporation of AA and β-GP could induce osteogenic gene expression at a relative high level, which provided a more suitable environment for osteogenic differentiation.

More importantly, the osteogenic effects in vivo is the key issue to evaluate the quality of tissue engineering scaffolds. Unfortunately, most of the currently designed bone tissue engineering scaffolds have limited osteogenic effects in vivo or not evaluated, which restricted the clinical transformation and application. In our current study, AA- and β-GP-modified biomimetic GH nanofibrous scaffolds can support BMSCs' growth and promote osteoblast differentiation and dramatically repair bone defect. It is exciting to find that the defect is almost totally repaired in the GH/A/B group within 6 weeks. Dual incorporation of AA and β-GP had burst the function of GH scaffolds. In vitro studies also indicated that dual incorporation of AA and β-GP could significantly stimulate *Alp* and *Col1* expressions. The crucial role of AA in the synthesis and posttranslational modification of collagen, as well as multiple functions of β-GP, can promote osteoblast differentiation and bone regeneration. AA and β-GP also showed synergistic effects on bone formation in vivo. Significantly, the results showed that the ends of GH/A/B scaffolds were embedded in the newly formed bone (red arrows show in Figure 7) and the newly formed bone that was deposited along with the surface of GH/A/B scaffold. This suggests that GH/A/B scaffold will serve as template for guiding bone formation. The GH/A/B scaffold creates a versatile microenvironment for osteoblast migration and differentiation. At 12 weeks, new bone formation was significantly improved in the GH, GH/A, and GH/B groups (Figure 7). GH/A and GH/B scaffolds also exibit considerable new bone formation. Among various implantation groups, the new bone became much more mature and bone deposition line became almost invisible at 12 weeks. The structure of newly formed lamellar bone was more similar to the native bone especially for the GH/A/B group. This may due to the remodeling of new bone after mineralization. Moreover, we could find some inflammatory cells infiltrated in the GH scaffold group. This may due to the aggregated HA nanoparticles that had been released from GH scaffold when degraded.[49] Fortunately, the incorporation of AA and β-GP can either suppress inflammation and immune responses, thus providing a more suitable environment for osteoblast proliferation and differentiation in vivo. However, the underlying mechanisms still need to be clarified. Collectively, our study demonstrates that GH/A/B scaffold provides a very convenient microenvironment for osteoblast proliferation and differentiation, which gives rise to new bone formation in vivo rapidly.

Conclusion

In the present study, AA and β-GP dual modified scaffold can repair 5-mm-critical sized cranial bone defects almost entirely within 6 weeks, thus serving as a template for guiding bone formation. Moreover, they can suppress inflammation and immune responses, consequentially providing a more suitable environment for osteoblast proliferation and differentiation. Our work highlights the importance of developing GH scaffolds for bone tissue engineering applications and, in particular, for the repair of nonunion critically sized defects.

Acknowledgment

This study was supported by the National Key Research and Development Program of China (2016YFC1102804 and 2016YFC1102803), the National Natural Science Foundation of China (81320108011, 81271111, 81600823, and 81600843), the Science Technology Program of Jilin Province (20170520009JH), and Postdoctoral Science Foundation (2017M611332 and 2017M621219).

Author contributions

All authors contributed to data analysis, drafting or revising the article, gave final approval of the version to be published, and agree to be accountable for all aspects of the work.

Disclosure

The authors report no conflicts of interest in this work.

References

1. Rose JC, De Laporte L. Hierarchical Design of Tissue Regenerative Constructs. *Adv Healthc Mater*. 2018;7(6):e1701067.
2. Burg KJ, Porter S, Kellam JF. Biomaterial developments for bone tissue engineering. *Biomaterials*. 2000;21(23):2347–2359.

3. Vas WJ, Shah M, Al Hosni R, Owen HC, Roberts SJ. Biomimetic strategies for fracture repair: Engineering the cell microenvironment for directed tissue formation. *J Tissue Eng*. 2017;8:2041731417704791.
4. Marcucio RS, Qin L, Alsberg E, Boerckel JD. Reverse engineering development: Crosstalk opportunities between developmental biology and tissue engineering. *J Orthop Res*. 2017;35(11):2356–2368.
5. Hynes RO. The extracellular matrix: not just pretty fibrils. *Science*. 2009;326(5957):1216–1219.
6. Vo TN, Shah SR, Lu S, et al. Injectable dual-gelling cell-laden composite hydrogels for bone tissue engineering. *Biomaterials*. 2016;83:1–11.
7. Wei G, Ma PX, Px M. Macroporous and nanofibrous polymer scaffolds and polymer/bone-like apatite composite scaffolds generated by sugar spheres. *J Biomed Mater Res A*. 2006;78(2):306–315.
8. Jariwala SH, Lewis GS, Bushman ZJ, Adair JH, Donahue HJ. 3D Printing of Personalized Artificial Bone Scaffolds. *3D Print Addit Manuf*. 2015;2(2):56–64.
9. Liu W, Thomopoulos S, Xia Y. Electrospun nanofibers for regenerative medicine. *Adv Healthc Mater*. 2012;1(1):10–25.
10. Xue J, Xie J, Liu W, Xia Y. Electrospun Nanofibers: New Concepts, Materials, and Applications. *Acc Chem Res*. 2017;50(8):1976–1987.
11. Buckwalter JA, Glimcher MJ, Cooper RR, Recker R. Bone biology. I: Structure, blood supply, cells, matrix, and mineralization. *Instr Course Lect*. 1996;45:371–386.
12. Kim HW, Song JH, Kim HE. Nanofiber generation of gelatin-hydroxyapatite biomimetics for guided tissue regeneration. *Adv Funct Mater*. 2005;15(12):1988–1994.
13. Kim HW, Kim HE, Salih V. Stimulation of osteoblast responses to biomimetic nanocomposites of gelatin-hydroxyapatite for tissue engineering scaffolds. *Biomaterials*. 2005;26(25):5221–5230.
14. Li D, Sun H, Jiang L, et al. Enhanced biocompatibility of PLGA nanofibers with gelatin/nano-hydroxyapatite bone biomimetics incorporation. *ACS Appl Mater Interfaces*. 2014;6(12):9402–9410.
15. Kim HW, Lee HH, Knowles JC. Electrospinning biomedical nanocomposite fibers of hydroxyapatite/poly(lactic acid) for bone regeneration. *J Biomed Mater Res A*. 2006;79(3):643–649.
16. Jaiswal AK, Chhabra H, Soni VP, Bellare JR. Enhanced mechanical strength and biocompatibility of electrospun polycaprolactone-gelatin scaffold with surface deposited nano-hydroxyapatite. *Mater Sci Eng C Mater Biol Appl*. 2013;33(4):2376–2385.
17. Zhao X, Han Y, Li J, et al. BMP-2 immobilized PLGA/hydroxyapatite fibrous scaffold via polydopamine stimulates osteoblast growth. *Mater Sci Eng C Mater Biol Appl*. 2017;78:658–666.
18. Niu B, Li B, Gu Y, Shen X, Liu Y, Chen L. In vitro evaluation of electrospun silk fibroin/nano-hydroxyapatite/BMP-2 scaffolds for bone regeneration. *J Biomater Sci Polym Ed*. 2017;28(3):257–270.
19. Hwang CJ, Vaccaro AR, Lawrence JP, et al. Immunogenicity of bone morphogenetic proteins. *J Neurosurg Spine*. 2009;10(5):443–451.
20. Pişkin E, Işoğlu IA, Bölgen N, et al. In vivo performance of simvastatin-loaded electrospun spiral-wound polycaprolactone scaffolds in reconstruction of cranial bone defects in the rat model. *J Biomed Mater Res A*. 2009;90(4):1137–1151.
21. Jiang L, Sun H, Yuan A, et al. Enhancement of osteoinduction by continual simvastatin release from poly(lactic-co-glycolic acid)-hydroxyapatite-simvastatin nano-fibrous scaffold. *J Biomed Nanotechnol*. 2013;9(11):1921–1928.
22. Yoon SJ, Park KS, Kim MS, Rhee JM, Khang G, Lee HB. Repair of diaphyseal bone defects with calcitriol-loaded PLGA scaffolds and marrow stromal cells. *Tissue Eng*. 2007;13(5):1125–1133.
23. Murphy CM, Schindeler A, Gleeson JP, et al. A collagen-hydroxyapatite scaffold allows for binding and co-delivery of recombinant bone morphogenetic proteins and bisphosphonates. *Acta Biomater*. 2014;10(5):2250–2258.
24. Chen J, He Y, Shan C, Pan Q, Li M, Xia D. Topical combined application of dexamethasone, vitamin C, and β-sodium glycerophosphate for healing the extraction socket in rabbits. *Int J Oral Maxillofac Surg*. 2015;44(10):1317–1323.
25. Franceschi RT, Iyer BS, Cui Y. Effects of ascorbic acid on collagen matrix formation and osteoblast differentiation in murine MC3T3-E1 cells. *J Bone Miner Res*. 1994;9(6):843–854.
26. Beck GR, Zerler B, Moran E. Phosphate is a specific signal for induction of osteopontin gene expression. *Proc Natl Acad Sci U S A*. 2000;97(15):8352–8357.
27. Beck GR Jr, Moran E, Knecht N. Inorganic phosphate regulates multiple genes during osteoblast differentiation, including Nrf2. *Exp Cell Res*. 2003;288(2):288–300.
28. Quarles LD, Yohay DA, Lever LW, Caton R, Wenstrup RJ. Distinct proliferative and differentiated stages of murine MC3T3-E1 cells in culture: an in vitro model of osteoblast development. *J Bone Miner Res*. 1992;7(6):683–692.
29. Wissink MJ, Beernink R, Pieper JS, et al. Immobilization of heparin to EDC/NHS-crosslinked collagen. Characterization and in vitro evaluation. *Biomaterials*. 2001;22(2):151–163.
30. Kuijpers AJ, Engbers GH, Krijgsveld J, Zaat SA, Dankert J, Feijen J. Cross-linking and characterisation of gelatin matrices for biomedical applications. *J Biomater Sci Polym Ed*. 2000;11(3):225–243.
31. Hashim DM, Man YBC, Norakasha R, Shuhaimi M, Salmah Y, Syahariza ZA. Potential use of Fourier transform infrared spectroscopy for differentiation of bovine and porcine gelatins. *Food Chem*. 2010;118(3):856–860.
32. Fl M, Shyu SS, Wong TB, Jang SF, Lee ST, Kt L. Chitosan–polyelectrolyte complexation for the preparation of gel beads and controlled release of anticancer drug. II. Effect of pH-dependent ionic crosslinking or interpolymer complex using tripolyphosphate or polyphosphate as reagent. *J Appl Polym Sci*. 1999;74(5):1093–1107.
33. Mwangi JW, Ofner CM 3rd. Crosslinked gelatin matrices: release of a random coil macromolecular solute. *Int J Pharm*. 2004;278(2):319–327.
34. Tajmir-Riahi HA. Coordination chemistry of vitamin C. Part II. Interaction of L-ascorbic acid with Zn(II), Cd(II), Hg(II), and Mn(II) ions in the solid state and in aqueous solution. *J Inorg Biochem*. 1991;42(1):47–55.
35. Pischetsrieder M, Larisch B, Muller U, Severin T. Reaction of ascorbic acid with aliphatic amines. *J Agric Food Chem*. 1995;43(12):3004–3006.
36. Schmitz OJ. DNA adducts as biomarkers for carcinogenesis analysed by capillary electrophoresis and laser-induced-fluorescence detection. In: Hering P, Lay JP, Stry S, editors. *Laser in Environmental and Life Sciences*. Berlin Heidelberg: Springer; 2004.
37. Meng ZX, Xu XX, Zheng W, et al. Preparation and characterization of electrospun PLGA/gelatin nanofibers as a potential drug delivery system. *Colloids Surf B Biointerfaces*. 2011;84(1):97–102.
38. Kuznetsova D, Ageykin A, Koroleva A, et al. Surface micromorphology of cross-linked tetrafunctional polylactide scaffolds inducing vessel growth and bone formation. *Biofabrication*. 2017;9(2):025009.
39. Guarino V, Veronesi F, Marrese M, et al. Needle-like ion-doped hydroxyapatite crystals influence osteogenic properties of PCL composite scaffolds. *Biomed Mater*. 2016;11(1):015018.
40. Englard S, Seifter S. The biochemical functions of ascorbic acid. *Annu Rev Nutr*. 1986;6:365–406.
41. Kadler KE, Baldock C, Bella J, Boot-Handford RP. Collagens at a glance. *J Cell Sci*. 2007;120(Pt 12):1955–1958.
42. Xing W, Pourteymoor S, Mohan S. Ascorbic acid regulates osterix expression in osteoblasts by activation of prolyl hydroxylase and ubiquitination-mediated proteosomal degradation pathway. *Physiol Genomics*. 2011;43(12):749–757.
43. Hadzir SN, Ibrahim SN, Abdul Wahab RM, et al. Ascorbic acid induces osteoblast differentiation of human suspension mononuclear cells. *Cytotherapy*. 2014;16(5):674–682.
44. Wilson CW. Clinical pharmacological aspects of ascorbic acid. *Ann N Y Acad Sci*. 1975;258:355–376.
45. Beck GR Jr. Inorganic phosphate as a signaling molecule in osteoblast differentiation. *J Cell Biochem*. 2003;90(2):234–243.
46. Nam HK, Liu J, Li Y, Kragor A, Hatch NE. Ectonucleotide pyrophosphatase/phosphodiesterase-1 (ENPP1) protein regulates osteoblast differentiation. *J Biol Chem*. 2011;286(45):39059–39071.

47. Okamoto T, Taguchi M, Osaki T, Fukumoto S, Fujita T. Phosphate enhances reactive oxygen species production and suppresses osteoblastic differentiation. *J Bone Miner Metab*. 2014;32(4):393–399.
48. Bianco P, Riminucci M, Gronthos S, Robey PG. Bone marrow stromal stem cells: nature, biology, and potential applications. *Stem Cells*. 2001;19(3):180–192.
49. Müller KH, Motskin M, Philpott AJ, et al. The effect of particle agglomeration on the formation of a surface-connected compartment induced by hydroxyapatite nanoparticles in human monocyte-derived macrophages. *Biomaterials*. 2014;35(3):1074–1088.